IFAC-PapersOnLine, Volume 50, Issue 1, 2017, Pages 2290-2295
DOI:10.1016/j.ifacol.2017.08.228

A Switching LOS Guidance with Relative Kinematics for Path-Following of Underactuated Underwater Vehicles

Bilal Abdurahman*. A. Savvaris. and A. Tsourdos.

*Cranfield University, School of Aerospace, Transport and Manufacturing, Cranfield, MK43 0AL UK (Tel: 01234-750111, ext.: 5022); email: a.bilale@cranfield.ac.uk).

Abstract: This paper presents a switching heuristic for the enclosure-based line-of-sight (ELOS) guidance and the concept of relative kinematics. The switching scheme proposed addresses the need for additional path-approaching strategies required in ELOS guidance in case of large cross-track errors. A nonlinear controller is applied to solve the path-following problem as a maneuvering problem, and the resulting guidance system with the relative kinematics perform well in compensating for drift caused by strong ocean currents. Stability and convergence analysis of the closed-loop systems are also provided along with simulation results showing straight-line waypoint-following performance of an AUV.

Keywords: path-following control, line-of-sight guidance, current compensation, underwater vehicles, AUVs

1. INTRODUCTION

Guidance systems play important roles in achieving control objectives such as path following and trajectory tracking for marine crafts including underwater vehicles (UVs). Path following is defined by a motion control scenario where the vehicle is required to follow a predefined path under no time constraints (Fossen, 2011). This paper will address an essential problem towards autonomous operations of UVs: path-following under ocean current disturbances along with redefined relative velocities. The lookahead-based line-of-sight (LLOS) guidance is a popular choice in design of path-following controllers, because it is simple and intuitive (see e.g. Healey and Lienard (1993), Børhaug et al. (2008), Lekkas and Fossen, (2009)). However, if there are no methods to counteract the effects of ocean currents in design, its performance is subject to severe degradation. The integral LOS designs have been common approaches to compensate for the drift caused by currents (for e.g. see Børhaug et al. (2008) and Breivik and Fossen (2009)).

The LOS guidance has two steering schemes: LLOS and enclosure-based LOS (ELOS). The LLOS scheme, also referred as traditional LOS, is computationally simpler than its ELOS counterpart. However, ELOS guidance intrinsically provides a varying *lookahead-distance* Δ, while Δ is constant in basic LLOS guidance. This distinct property of ELOS could be attributed to why it performs better than LLOS when following curved paths (see carrot-chasing guidance and the nonlinear guidance law in Sujit et.al., 2014). The ELOS scheme creates an enclosing circle around the vehicle with a fixed radius R, and one of this circle-path interceptions is used to generate the LOS angle ψ_{los} for desired heading (Fossen et.al., 2003). It is critical for R to be greater than the cross-track error $|y_e|$, so that the circle-path interceptions exist, which includes waypoint-following scenarios such that $R \geq R_k$, where R_k is radius of the *circle of acceptance* at k^{th} way-point. Thereby, it is required that $R \geq |y_e|$ for all y_e in general. R is tuned accordingly in practice, normally as n ship-length L_{pp} . While the existence of circle-path interceptions can be ensured by choosing a sufficiently large radius, a large R will project a Δ too far ahead of the vehicle, resulting in a longer path convergence time. A smaller R produces a steeper ψ_{los} and thus can decrease the path convergence time, and a path approaching strategy has to be in place when there are no circle-path interceptions, i.e. when $|y_e| > R$. To overcome this drawback, Moreira et.al. (2007) proposed to increase R linearly with y_e , and Khaled and Chalhoub (2013) proposed to increase it exponentially with d, while the later achieved a faster path convergence.

A switching scheme is proposed for the ELOS guidance to overcome the above drawback in this paper. The idea of relative kinematics is also introduced which separates the relative velocities into inertial and FLOW reference frames. The ocean current is compensated directly using sideslip feedback. The resulting guidance is applied in a 2-D waypoint-following scenario using the model of Girona-500 AUV and can also be applied to a range of other systems. A nonlinear controller is applied during path-following, and stability and convergence analysis, and simulation results are also provided at the end.

2. SYSTEM MODEL AND ONTROL OBJECTIVE

2.1 System Model

The system model consists of the horizontal motion of underwater vehicles that can be described by the decoupled 3-DOF model (Fossen, 2011):

$$\dot{\boldsymbol{\eta}} = \boldsymbol{R}(\psi)\boldsymbol{v} \tag{1}$$

$$\boldsymbol{M}\dot{\boldsymbol{v}} + \boldsymbol{C}(\boldsymbol{v})\boldsymbol{v} + \boldsymbol{D}(\boldsymbol{v})\boldsymbol{v} + \boldsymbol{g}(\boldsymbol{\eta}) = \boldsymbol{B}\boldsymbol{f} \tag{2}$$

where $\boldsymbol{\eta} \triangleq [x, y, \psi]^T$ is the horizontal position and orientation of the vehicle in inertial frame i, and $\boldsymbol{v} \triangleq [u, v, r]^T$ is the vector of absolute velocities of the vehicle in

surge, sway, and yaw in body-fixed frame b, and $\boldsymbol{R}(\psi)$ is the transformation matrix from b to i. Furthermore, $\boldsymbol{M} = \boldsymbol{M}^T > 0$ is the system mass-inertia matrix including added mass, $\boldsymbol{C}$ is the Coriolis and centripetal matrix including rigid-body and added-mass terms, $\boldsymbol{D} > 0$ is the damping matrix including linear and quadratic terms, $\boldsymbol{g}(\boldsymbol{\eta}) \triangleq [0\ 0\ 0]^T$ is the gravitational and restoring forces and moments. The control input vector $\boldsymbol{M^{-1}Bf} \triangleq [\tau_u, 0, \tau_\psi]^T$ consists of surge thrust and yaw moment, where $\boldsymbol{f} \in \mathcal{R}^2$ is the actuator input vector and $\boldsymbol{B} \in \mathcal{R}^{3\times 2}$ is the actuator configuration matrix. This structure of the control input vector is obtained by assuming that b is positioned in the pivot point such that yaw moment has no effect on sway motion (Fredriksen and Pettersen). Note that system (2) is underactuated since the dimension of $\boldsymbol{f}$ is less than that of the system.

The relative velocities are defined as follows. The relative velocities of the vehicle relative to i frame $\boldsymbol{v}_r^i$ is

$$\boldsymbol{v}_r^i \triangleq \boldsymbol{v} + \boldsymbol{\upsilon}_c = [u_r^i, v_r^i, r_r^i]^T \tag{3}$$

where $\boldsymbol{\upsilon}_c \triangleq [u_c, v_c, 0]^T$ is the ocean current velocity in b. The relative velocities of the vehicle relative to FLOW frame $\boldsymbol{v}_r^f$ is

$$\boldsymbol{v}_r^f \triangleq \boldsymbol{v} - \boldsymbol{\upsilon}_c = \left[u_r^f, v_r^f, r_r^f\right]^T \tag{4}$$

Current velocities u_c and v_c are given by: $u_c = V_c \cos(\beta_c - \psi)$, $v_c = V_c \sin(\beta_c - \psi)$, where $V_c \triangleq \sqrt{u_c^2 + v_c^2} > 0$ and $\beta_c = \text{atan2}(V_y, V_x)$ are the current intensity and heading in i, and $\boldsymbol{V}_c \triangleq \left[V_x, V_y, 0\right]^T$ is the ocean current velocity in i. The ocean current is assumed constant (slowly-varying) and irrotational in i, which gives $\dot{\boldsymbol{V}}_c = \boldsymbol{0}$ and $\dot{\boldsymbol{\upsilon}}_c = [r_r^i v_c, -r_r^i u_c, 0]^T$. Since the relative velocities are defined differently at kinetic and kinematic levels, (3) and (4) are substituted into (1) and (2), respectively, which gives the relative equations of motion as:

$$\dot{\boldsymbol{\eta}} = \boldsymbol{R}(\psi)\boldsymbol{v}_r^i \tag{5}$$

$$\boldsymbol{M}\dot{\boldsymbol{v}}_r^f + \boldsymbol{C}\left(\boldsymbol{v}_r^f\right)\boldsymbol{v}_r^f + \boldsymbol{D}\left(\boldsymbol{v}_r^f\right)\boldsymbol{v}_r^f + \boldsymbol{g}(\boldsymbol{\eta}) = \boldsymbol{Bf}. \tag{6}$$

Expanding (5) gives

$$\dot{x} = u_r^i \cos\psi - v_r^i \sin\psi \tag{7}$$
$$\dot{y} = u_r^i \sin\psi + v_r^i \cos\psi \tag{8}$$
$$\dot{\psi} = r_r^i \tag{9}$$

Remark 1. The definitions of relative velocities in (3) and (4) have to be different because they are relative to different reference frames, i.e. a velocity relative to the inertial frame is different than a velocity relative to the FLOW frame. The kinetics model (6) is a common model as in (Fossen, 2012).

The system matrices then take the following structure:

$$\boldsymbol{M} \triangleq \begin{bmatrix} m_{11} & 0 & 0 \\ 0 & m_{22} & m_{23} \\ 0 & m_{23} & m_{33} \end{bmatrix}, \tag{10}$$

$$\boldsymbol{C}\left(\boldsymbol{v}_r^f\right) \triangleq \begin{bmatrix} 0 & 0 & c_{13}\left(r_r^f, v_r^f\right) \\ 0 & 0 & c_{23}\left(u_r^f\right) \\ -c_{13}\left(r_r^f, v_r^f\right) & -c_{23}\left(u_r^f\right) & 0 \end{bmatrix}. \tag{11}$$

$$\boldsymbol{D}\left(\boldsymbol{v}_r^f\right) \triangleq \text{diag}\{d_{11}\left(u_r^f\right), d_{22}\left(v_r^f\right), d_{33}\left(r_r^f\right)\}, \tag{12}$$

The particular structure for in system matrices (10-11) are obtained by assuming that the vehicle is symmetric in port-starboard, and that the body-fixed coordinate system is located along the centre-line of the vehicle (Fossen, 2011). The dynamics of the vehicle relative to FLOW frame is obtained by expanding (6):

$$\dot{u}_r^f = -\frac{1}{m_{11}}\left(c_{13} r_r^f + d_{11} u_r^f - \tau_u\right), \tag{13}$$

$$\dot{v}_r^f = -\frac{1}{m_{22}}\left(c_{23} r_r^f + d_{22} v_r^f\right) - m_{23}\dot{r}_r^f, \tag{14}$$

$$\dot{r}_r^f = \frac{1}{m_{33}}\left(c_{13} u_r^f + c_{23} v_r^f - d_{33} r_r^f + \tau_\psi\right) - m_{23}\dot{v}_r^f. \tag{15}$$

where the arguments for elements of $\boldsymbol{C}$ and $\boldsymbol{D}$ are omitted. Note that the yaw component of the ocean current $V_r = r_c = 0$ since it is irrotational in i, and thus, $r_r^i = r_r^f = r$.

2.2 Control Objective

The path following problem is solved as a manoeuvring problem (Fossen, 2003), where the horizontal relative speed $U_{hr}^i \triangleq \sqrt{{u_r^i}^2 + {v_r^i}^2}$ of the vehicle in i converges to and follows a predefined straight-line path at a desired horizontal relative speed $U_{hdr}^i \geq V_c > 0$ along the path, which is defined as

$$U_{hdr}^i \triangleq \sqrt{{u_{dr}^i}^2 + {v_{dr}^i}^2} \triangleq \sqrt{(u_d + u_c)^2 + (v_d + v_c)^2}, \tag{16}$$

where u_{dr}^i and v_{dr}^i are the desired relative surge and sway velocities in i, and u_d and v_d are the desired absolute surge and sway velocities. Since sway DOF is not actuated, $v_d = 0$, and from (16)

$$v_{dr}^i = \sqrt{{U_{dr}^i}^2 + {u_{dr}^i}^2} = v_c, \tag{17}$$

$$u_{dr}^i = \sqrt{{U_{hdr}^i}^2 - {v_c}^2}. \tag{18}$$

The control objectives are then formulized as follows:

$$lim_{t\to\infty}\, u_r^i(t) = u_{dr}^i(t), \tag{19}$$

$$lim_{t\to\infty}\, \psi(t) = \psi_{crs}(t), \quad \psi_{crs} \in \left(-\frac{\pi}{2}, \frac{\pi}{2}\right), \tag{20}$$

$$lim_{t\to\infty}\, y_e(t) = 0. \tag{21}$$

where ψ_{crs} is the desired course angle and y_e is the cross-track error. The inertial coordinate system i can be placed along the x-axis of the desired path with path-frame P such that the y position of the vehicle becomes the cross-track error y_e.

Control of relative velocities instead of absolute velocities provides better energy efficiency since the hydrodynamic damping depends on $\boldsymbol{v}_r^f$ and the vehicle can benefit from the current velocities without actuator effort when β_c coincides with ψ_{crs}.

3. ELOS GUIDANCE

The reference $p_{los} = (x_{los}, y_{los})$ for ELOS is found by solving the following two equations with two unknowns:

$$(x_{los} - x)^2 + (y_{los} - y)^2 = R^2, \quad (22)$$

$$\frac{y_{los}-y_k}{x_{los}-x_k} = \frac{y_{k+1}-y_k}{x_{k+1}-x_k} = \tan\alpha_k = \text{constant}. \quad (23)$$

Once p_{los} is projected, ψ_{los} is given by

$$\psi_{los} \triangleq \tan^{-1}\left(\frac{y_{los}-y}{x_{los}-x}\right) = \tan^{-1}\left(\frac{-y_e}{\Delta}\right), \quad (24)$$

where the later equality is obtained by placing the *i*-frame onto *P*-frame, which resembles the LLOS scheme. It is critical for R to be sufficiently large so that solutions to (22) exist, i.e. $R \geq |d|$ and R is constant in this scheme.

3.1 Linearly and Exponentially Varying R

The linearly varying R proposed in Moreira et.al. (2007) calculates the LOS coordinates (x_{los}, y_{los}) as

$$(x_{los} - x)^2 + (y_{los} - y)^2 = R^2 = (L_{pp} + y_e)^2, \quad (25)$$

where R is a linear function of y_e. In the exponentially varying scheme, R is computed as (Khaled and Chalhoub, 2013)

$$R = y_e + \sqrt{2}R'_{min}e^{-dx'_B}, \quad (26)$$

$$R'_{min} = 2^{-0.5}R_{min}e^{2^{-0.5}dR_{min}}, \quad (27)$$

$$x'_B = d^{-1}\left[lambertw\left(R'_{min}e^{-(0.5\sqrt{2}dy_e)}\right) + 0.5\sqrt{2}by_e\right], \quad (28)$$

where the Lambert-W function is inverse of $f(x) = xe^x$, $R_{min} = nL_{pp}$, and d is the rate of decay for the exponential term. The equations for exponentially varying scheme lead to $R \cong y_e$ for large y_e, creating a circle tangent to the desired path. This results in a perpendicular path approaching angle for ψ_d, which is a natural strategy to pursue the shortest path between the current vehicle position and desired path. The exponential term dominated the value of R for small values of y_e, which ensured that R is increased at a lower rate compared to the linearly varying scheme $(R = R_{min} + y_e)$. This can keep the value of R small at lower values of y_e, which, as mentioned earlier, provides a steeper angle for ψ_d that can improve the path convergence rate of the vehicle (Khaled and Chalhoub, 2013).

4. SWITCHING ELOS GUIDANCE

In the switching ELOS (SELOS) scheme proposed, R is varied linearly on a conditional base, that is

$$R = \begin{cases} R_{min} & if\ |y_e| < R_{min} \\ a|y_e| & if\ |y_e| > R_{min} \end{cases}, \quad (29)$$

where $a \geq 1$ is a design constant, which determines the path approaching strategy outside $R_{\min}$. As can be seen, R is a function of y_e only when $|y_e|$ is greater than $R_{\min}$, preventing y_e from entering the guidance law, and thus preserving the properties of ELOS inside $R_{\min}$. This is not the case for both linearly or exponentially varying schemes where R is always a function of y_e. Equation (29) also guarantees circle-path interceptions always exist since for $a \geq 1$, $R \geq |y_e|$. The following two cases are used to explain (29).

Case 1: $(|y_e| < R_{\min})$. The guidance is the same as ELOS.
Case 2: $(|y_e| \geq R_{\min})$. If $a = 1$, $R = |y_e|$. This implies that ψ_d for path approaching is perpendicular to the path, corresponding to a shortest-path strategy, which is always guaranteed for ψ_d if $1 \leq a \approx 1$, with an enclosing circle tangent to the path.

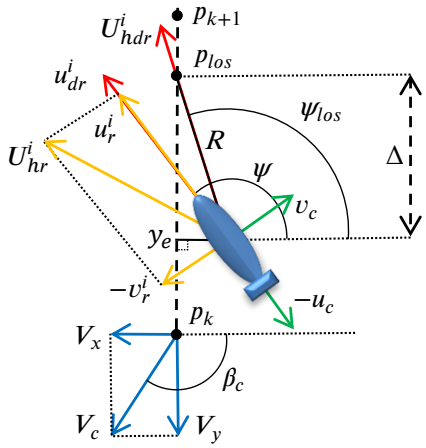

Fig. 1. Geometry of ELOS guidance and velocity vectors

4.1 Tuning R_{min}

$R_{\min}$ is chosen in a similar way as nL_{pp} and in general, smaller $R_{\min}$ could be preferred which project shorter Δ and thus faster path convergence time. Particularly, the lower bound for $R_{\min}$ is not limited or affected by y_e as opposed the linearly or exponentially varying schemes. The ELOS guidance corresponds to the LLOS guidance by a time-varying $\Delta(t) = \sqrt{R^2 - y_e{}^2}$. If Δ is too small, it corresponds to a large proportional action which results in an aggressive steering (Fossen, 2011), and this also applies to ELOS guidance. Nevertheless, the notion of aggressive steering described in (Fossen, 2011) is more applicable when both Δ and $|y_e|$ are small, which represents a case where the vehicle is very close to the path but the desired heading is still near perpendicular to it. In this case, if the aggressive steering required is not provided by the actuators, the vehicle may fly across the path without being able to turn towards an adequate Δ ahead if it is travelling at a sufficient forward speed. This can result in an oscillating behaviour. On the other hand, if Δ is small but $|y_e|$ is large, the vehicle is far away from the path and a perpendicular desired heading is projected, which may not imply an aggressive steering but a shortest-path strategy. Therefore, a small Δ is desired when the vehicle is far away from the path to achieve the shortest-path strategy, and a larger Δ is desired when the vehicle is close to the path to avoid an aggressive steering. This is an intrinsic path following strategy provided by ELOS guidance — provision of a varying Δ, which is achieved by both the exponentially varying and the switching schemes. As mentioned earlier, the steering required may become aggressive if the actuators cannot provide the required steering. Thus, the minimum allowable radius for $R_{\min}$ depends on vehicle actuators and can be a lower-saturated function of actuator constraints.

4.2 Continuous SELOS

The discontinuity in (29) is not desirable. A continuous approximation using a sigmoid function can be used to smooth out the discontinuity, which is given by

$$R = R_{\min} + \frac{1}{2}\left[\frac{(a|y_e| - R_{\min})(|y_e| - R_{\min})}{c + ||y_e| - R_{\min}|} + a|y_e| - R_{\min}\right] \quad (30)$$

where $1/c > 0$ is the slope of the sigmoid function at the origin. For a small c, (30) becomes

$$R \approx \begin{cases} R_{\min} & if\ |y_e| < R_{\min} \\ a|y_e| & if\ |y_e| > R_{\min} \end{cases}. \quad (31)$$

Fig. 2 shows the difference between the SELOS and the other two schemes on how ψ_{los} is produced over the range of $|d|$. The gains are set as $R_{\min} = 3$, $a = 1$, $d = 0.05$ and $c = 0.01$. It shows that SELOS reaches the $R = |y_e|$ slope representing the shortest-path as soon as $|y_e| > R_{\min}$, while the exponentially varying scheme reaches it very slowly, producing less steep ψ_{los} and hence, slower path convergence. The linearly varying scheme does not reach the line $R = |y_e|$, and hence does not provide a shortest-path strategy.

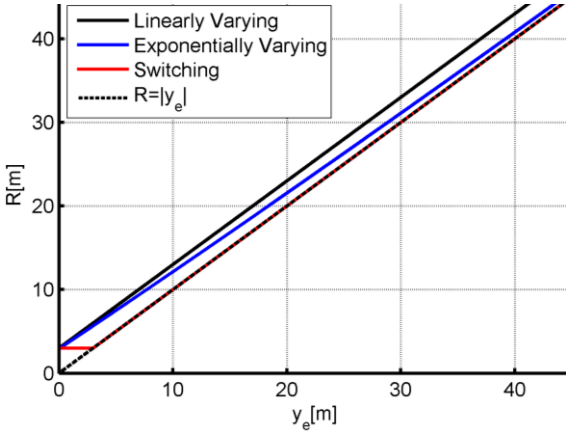

Fig. 2. Tuning schemes for varying R over y_e.

Remark 2. It should be noted that higher values for d can improve the convergence rate of the exponentially varying scheme to the slope $R = |y_e|$, but this results in an initial R being lower than $R_{\min}$, which does not give a solution to the ELOS guidance. Therefore, the maximum value of d could only be set to 0.05.

5. CONTROLLER

5.1 Sideslip Compensation

In the presence of ocean current the vehicle must be allowed to sideslip to counteract the effect of the current. Assuming the relative velocities in *i* are available, direct feedback of the sideslip angle β and sufficient actuation can compensate for the drift caused by ocean currents. The sideslip angle in this case is given by:

$$\beta \triangleq atan2\left(\frac{v_r^i}{u_r^i}\right). \quad (32)$$

This gives the desired course angle as

$$\psi_{crs} \triangleq \psi_d - \beta = \psi_{los} - \beta, \quad (33)$$

where $\psi_d = \psi_{los}$, which is given by the SELOS guidance (22-24) and (30).

5.2 Yaw Control

The yaw angle ψ of the vehicle is controlled towards ψ_{crs} as in control objective (20). The yaw error dynamics are defined as $\tilde{\psi} \triangleq \psi_{crs} - \psi$ and $s \triangleq \dot{\tilde{\psi}} + \lambda\tilde{\psi}$, where $\lambda > 0$ is controller bandwidth. Taking the time-derivative of $\tilde{\psi}$ and s and using system dynamics in (3) and (15) gives

$$\dot{\tilde{\psi}} = \dot{\psi}_{crs} - r_r^i \quad (34)$$

$$\begin{aligned} \dot{s} &= \ddot{\tilde{\psi}} + \lambda\dot{\tilde{\psi}} \\ &= \ddot{\psi}_{crs} - \frac{1}{m_{33}}\left(c_{13}u_r^f + c_{23}v_r^f - d_{33}r_r^f + \tau_\psi\right) \\ &\quad + m_{23}\dot{v}_r^f + \lambda\left(\dot{\psi}_{crs} - r_r^i\right). \end{aligned} \quad (35)$$

The sliding controller for yaw is given by:

$$\begin{aligned} \tau_\psi = {} & c_{13}u_r^f + c_{23}v_r^f - d_{33}r_r^f \\ & + m_{33}\left[\ddot{\psi}_{crs} + \lambda\left(\dot{\psi}_{crs} - r_r^i\right) + m_{23}\dot{v}_r^f + k_\psi\tilde{\psi} + k_d s\right], \end{aligned} \quad (36)$$

where $k_d, k_\psi > 0$ are constant gains. The time-derivative of an LFC $V_\psi \triangleq (1/2)k_\psi\tilde{\psi}^2 + (1/2)s^2$ is considered for stability analysis of the dynamics (34-35), that is

$$\dot{V}_\psi = -\lambda k_\psi\tilde{\psi}^2 - k_d s^2 \leq 0. \quad (37)$$

Since $\dot{V}_\psi$ is negative definite, the origins $(\tilde{\psi}, s) = (0,0)$ is UGES, and hence, $(\tilde{\psi}, s) \to (0,0)$ exponentially as $t \to \infty$. This satisfies the control objective (20). Notice that exponential convergence of $(\tilde{\psi}, s) \to (0,0)$ implies exponential convergence of $r_r^i \to \dot{\psi}_{crs}$ since $s - \lambda\tilde{\psi} = \dot{\psi}_{crs} - r_r^i$, and hence, $\dot{\tilde{\psi}} \to 0$. The reference signals $\dot{\psi}_{crs}$, $\ddot{\psi}_{crs}$ are obtained by

$$\dot{\psi}_{crs} = k_r(\psi_{crs} - \psi) = k_r\tilde{\psi}, \quad (38)$$

$$\ddot{\psi}_{crs} = k_a\left(\dot{\psi}_{crs} - \dot{\psi}\right) = k_a\dot{\tilde{\psi}}, \quad (39)$$

where $k_r, k_a \geq 0$ are constant gains. In order to prevent jumps in ψ_{crs} (e.g. during way-point switching) the following integration is used to obtain small increments for ψ_{crs}

$$\psi_{crs} = \psi + \dot{\psi}_{crs}T_s = \psi + k_r T_s\tilde{\psi}, \quad (40)$$

where T_s is the integrator sampling time. Note that $\tilde{\psi} \to 0$ also implies $\psi \to \psi_{crs}$ in (40).

5.3 Surge Control

The relative surge velocity u_r^i is controlled towards the desired relative surge velocity u_{dr}^i, which is generated by (18). The error in surge in *i* is defined as $\tilde{u}_r^i \triangleq u_{dr}^i - u_r^i$, and using (3-4) and (13) its dynamics is given by

$$\begin{aligned} \dot{\tilde{u}}_r^i &\triangleq \dot{u}_{dr}^i - \dot{u}_r^i = \dot{u}_{dr}^i - (\dot{u}_r^f + 2\dot{u}_c) \\ &= \dot{u}_{dr}^i + \frac{1}{m_{11}}\left(c_{13}r_r^f + d_{11}u_r^f - \tau_u - 2rv_c\right). \end{aligned} \quad (41)$$

The control law for surge is given by

$$\tau_u = c_{13}r_r^f + d_{11}u_r^f + m_{11}\left(\dot{u}_{dr}^i + k_u\tilde{u}_r^i\right), \quad (42)$$

where $k_u > 0$ is constant gain, and the desired relative surge acceleration $\dot{u}_{dr}^i$ is then given by:

$$\dot{u}_{dr}^i = k_1 \tilde{u}_r^i. \tag{43}$$

Controller (42) is a feedback linearizing proportional control that depends on relative and current velocities. Stability of system (41) is analysed using the time-derivative of the CFL $V_u \triangleq (1/2){\tilde{u}_r^i}^2$, which is

$$\dot{V}_u = -k_u {\tilde{u}_r^i}^2 \leq 0. \tag{44}$$

$\dot{V}_u$ is negative definite and hence, the origin of (41) is UGES, which means $\tilde{u}_r^i(t) \to 0$ exponentially as $t \to \infty$. This satisfies control objective (19).

5.4 Cross-Track and Sway Error Dynamics

The cross-track error dynamics $\dot{y}_e$ can be described by the sway dynamics in (8). Using the expressions $u_r^i = u_{dr}^i - \tilde{u}_r^i$, $\psi = \psi_{crs} - \tilde{\psi}$, (3-4) (14-15) and (32-33), $\dot{y}_e$ is given as the following when $\tilde{\psi} = 0$ and $\tilde{u}_r^i = 0$:

$$\dot{y}_e = u_{dr}^i \sin(\psi_{crs}) - v_r^i \cos(\psi_{crs}), \tag{45}$$

which can be written in phase-amplitude form as

$$\dot{y}_e = \sqrt{{u_{dr}^i}^2 + {v_r^i}^2} \sin\left(\psi_{crs} + \tan^{-1}\left(\frac{v_r^i}{u_{dr}^i}\right)\right) \tag{46}$$

Substituting $u_r^i = u_{dr}^i - \tilde{u}_r^i$ into (32) and using (33), (46) becomes

$$\dot{y}_e = \sqrt{{u_{dr}^i}^2 + {v_r^i}^2} \sin\left(\frac{-y_e}{\sqrt{\Delta^2 + {y_e}^2}}\right) \tag{47}$$

Proposition 1. For $\sqrt{{u_{dr}^i}^2 + {v_r^i}^2}$, $\Delta > 0$, the origin $y_e = 0$ of system (47) is globally κ-exponentially stable.

Proof: The proof is similar to that in (Lekkas and Fossen, 2013). It was first shown by (Pettersen and Leffeber, 2001). ■

Thus, from Proposition 1, $y_e \to 0$ asymptotically as $t \to \infty$, satisfying objective (21).

The sway error in i is defined as $\tilde{v}_r^i \triangleq v_{dr}^i - v_r^i = v_c - v_r^i$. Using (3-4) and (14-15), (17), (36), (38-39) the sway error dynamics is given by and simplified to

$$\begin{aligned}\dot{\tilde{v}}_r^i &= 3\dot{v}_c - \dot{v}_r^f \\ &= \frac{2m_{23}}{\alpha m_{33}}\left(c_{13}u_r^f + c_{23}v_r^f\right) + \frac{d_{22}}{\alpha m_{22}}(v_r^i - 2v_c) - \\ &\quad - \frac{m_{23}}{\alpha}\left[\left(\frac{c_{23}}{m_{23}m_{22}} - \frac{2d_{22}}{m_{33}} - k_a - k_d - \lambda + 3u_c\right)\dot{\tilde{\psi}} - \right. \\ &\quad \left. - \left(k_\psi + k_d\lambda - \frac{2d_{33}k_r}{m_{33}} - \frac{3\alpha k_r u_c}{m_{23}}\right)\tilde{\psi}\right],\end{aligned} \tag{48}$$

where $\alpha = 1 + m_{23} + m_{23}^2$.

Proposition 2. The origin of the closed-loop sway system (48) is UGAS if the following condition is satisfied:

$$\frac{d_{22}}{m_{22}} > \frac{v_r^i v_c}{\left({v_r^i}^2 + 2v_c^2\right)m_{33}}\left[3d_{22} - 2m_{23}\left(\frac{c_{23}v_r^f}{v_c} - c_{13}u_r^f\right)\right]. \tag{49}$$

Proof: It is shown that $(\tilde{\psi}, \dot{\tilde{\psi}}) \to (0,0)$ exponentially, and thus, using the cascaded approach as in (Pettersen and Leffeber, 2001), it is left to verify that the following system reduced from (48) is UGAS when $\tilde{\psi}$ and $\dot{\tilde{\psi}}$ are zero, which is

$$\dot{\tilde{v}}_r^i = \frac{2m_{23}}{\alpha m_{33}}\left(c_{13}u_r^f + c_{23}v_r^f\right) + \frac{d_{22}}{\alpha m_{22}}(v_r^i - 2v_c). \tag{50}$$

The time-derivative of a CFL $V_v \triangleq (1/2){\tilde{v}_r^i}^2$ for (50) is then given by

$$\begin{aligned}\dot{V}_v &= \frac{v_r^i}{\alpha m_{33}}\left(3d_{22}v_c - 2m_{23}c_{23}v_r^f\right) - \frac{d_{22}}{\alpha m_{22}}\left({v_r^i}^2 + 2v_c^2\right) \\ &\quad + \frac{2m_{23}c_{13}u_r^f v_c}{\alpha m_{33}}.\end{aligned} \tag{51}$$

It can be seen that $\dot{V}_v$ is negative definite if

$$\frac{d_{22}}{m_{22}} > \frac{v_r^i v_c}{\left({v_r^i}^2 + 2v_c^2\right)m_{33}}\left[3d_{22} - 2m_{23}\left(\frac{c_{23}v_r^f}{v_c} - c_{13}u_r^f\right)\right]. \tag{52}$$

Therefore, if the inequality (52) is satisfied, the origin of (48) is UGAS. Thus, $\dot{\tilde{v}}_r^i \to 0$ asymptotically as $t \to \infty$. ■

6. SIMULATION RESULTS

Simulations were carried out using the model of Girona-500 AUV in way-point following scenarios with a constant current disturbance of $V_c = 1\ m/s$ from Northeast direction. The vehicle parameters were obtained from (Karras et.al., 2013). The initial conditions and desired states are set as $\boldsymbol{\eta}_o = [4,5,0]^T$, $\boldsymbol{v}_{ro}^f = \boldsymbol{v}_{ro}^i = [0,0,0]^T$, $U_{hdr}^i = 1\ m/s$. The gains for guidance and controller are as: $R_k = 0.8$, $R_{min} = 0.8$, $a = 1.001$, $c = 0.001$, $\lambda = 120$, $k_d = 25, k_r = k_a = k_\psi = k_1 = 1, k_u = 25$. The waypoints used are: $wpx = \{10, 14, 21, 26, 32\}$, $wpy = \{5, 22, 22, 8, 17.5\}$.

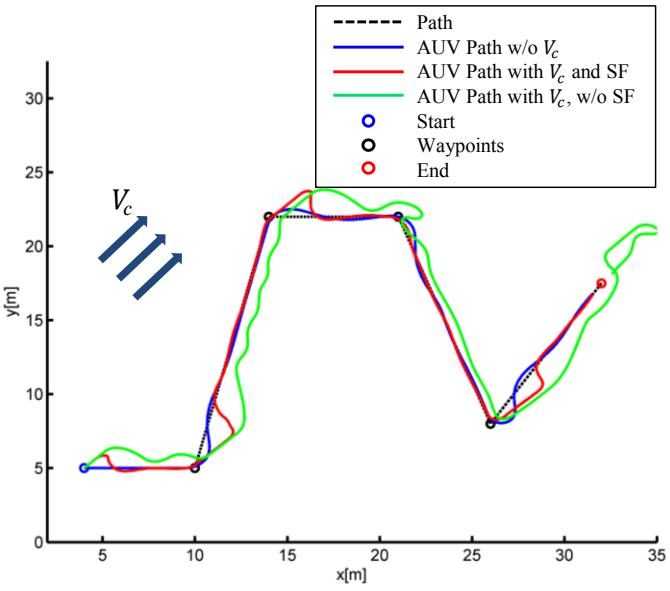

Fig. 3. Waypoint following with current disturbance at $\beta_c = \pi/4$ and $V_c = 1\ m/s$.

Path-following performance of SELOS guidance with sideslip feedback with and without current disturbances from Northeast direction is shown in Fig. 3. It shows that the SELOS controller renders the vehicle to accurately follow the path in both cases if there is sideslip feedback (SF). The AUV cannot follow the path under disturbance if there is no SF, emphasizing the importance of SF. Fig. 4. Shows the

velocity tracking profiles, where it shows that U_{hdr}^{i}, u_{dr}^{i} and v_{dr}^{i} are accurately tracked except for U_{hdr}^{i} and u_{dr}^{i} when there are strong currents in adverse direction, especially during the fourth segment of the path, around time interval from 40 to 60 seconds. This is because the control inputs are designed saturate at $\pm 350\ N$, thus the vehicle is unable to provide sufficient actuation to overcome the adverse current. This is to make the simulation describe a more realistic behaviour. Fig. 6 shows that heading ψ closely tracks ψ_{crs} and the cross-track error is kept near zero except during turning at waypoints. The program treats the initial position to the first waypoint as the zeroth waypoint, which is why the cross-track error starts at zero.

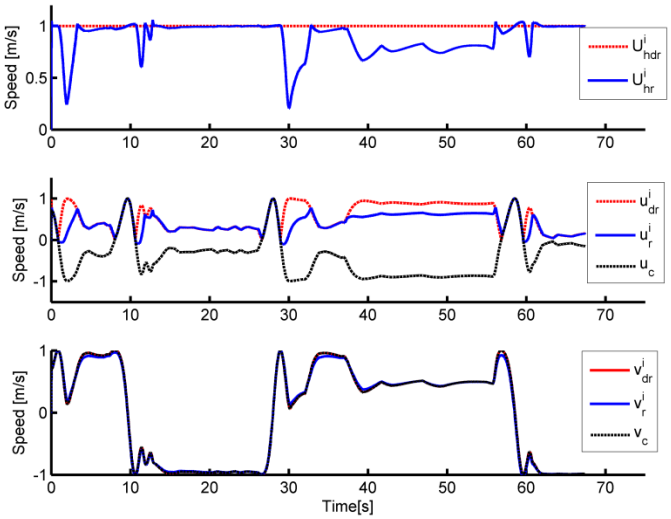

Fig. 5. Velocity and heading tracking during path-following with current disturbance of $\beta_c = \pi/4$ and $V_c = 1\ m/s$.

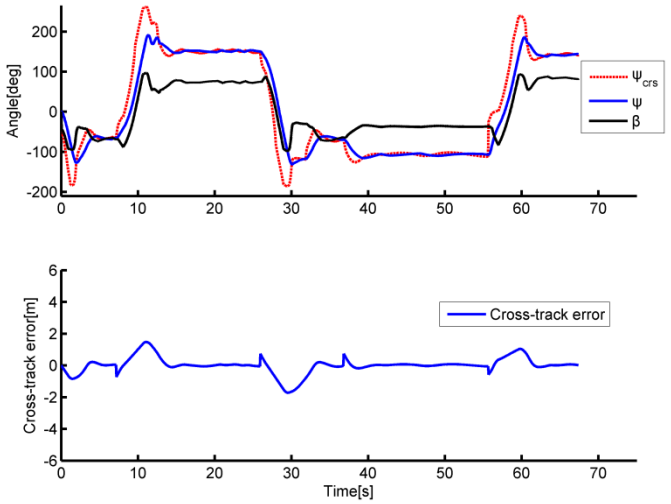

Fig. 6. Heading angles and cross-track error during path-following at $\beta_c = \pi/4$ and $V_c = 1\ m/s$.

7. CONCLUSION

A switching mechanism for ELOS guidance is presented in this paper, which meets the requirement for having extra path-approaching strategies in case of large cross-track errors for ELOS guidance. It is shown that the switching scheme is simpler and produces better path-approaching angles compared to the linearly and exponentially varying schemes and achieves shorter path convergence time. The idea of relative kinematics is also introduced to define the relative velocities at the kinetic and kinematic levels separately. A nonlinear controller is applied during path-following and stability and convergence analysis are provided for the closed-loop error dynamics. Simulation results showed that the resulting guidance and the relative kinematics model enable an AUV to accurately track a 2D path consisting of straight-lines under strong current disturbances. The concept of relative kinematics can also be extended to describe the relative motion of systems other than underwater vehicles.

REFERENCES

Børhaug, E., Pavlov, A. and Pettersen, K.Y. (2008). Integral LOS control for path following of underactuated marine surface vessels in the presence of constant ocean currents. In *Proc. of the 47th IEEE Conference on Decision and Control*, 4984–4991.

Breivik, M. and Fossen, T.I. (2009). *Guidnace Laws for Autonomous Underwater Vehicles*, ch. 4, 51–76. A.V., Inzartsev, IN-TECK Education and Publishing.

Fossen, T.I. (2011). *Handbook of marine craft hydrodynamics and motion control.* John Wiley and Sons Ltd., Chichester, UK.

Fossen, T.I. (2012). How to incorporate wind, waves and ocean currents in the marine craft equations of motion. In *Proc. of the 9th IFAC Conference on Manoeuvring and Control of Marine Craft,* 126–131.

Fossen, T. I., Breivik M., and Skjetne, R. (2003). Line-of-sight path following of underactuated marine craft. In *Proc. of the 6th IFAC Conference on Manoeuvring and Control of Marine Craft*, 244–249.

Healey, A.J. and Lienard, D. (1993). Multivariable sliding mode control for autonomous diving and steering control of autonomous underwater vehicles. In *IEEE J. Oceanic Eng.*, vol. 18(3), 327–339.

Karras G.C., Bechlioulis, C.P., Leonetti, M., Palomeras, N., Kormushev, P., Kyriakopoulos, K.J. and Caldwell, D.J. (2013). On-line Identification of autonomous underwater vehicles through global derivative-free optimization. In *Proc. of IEEE/RSJ International Conference on Intelligent Robots and Systems,* 3859–3864.

Khaled, N. and Chalhoub, N.G. (2013). A self-tuning guidance and control system for marine surface vessels. *Nonlinear Dynamics*, 73(1), 897–906.

Lekkas, A.M. and Fossen, T.I. (2013). *Line-of-sight guidance for path following of marine vehicles,* ch. 5, 63–92, Gal, O., Lamber Academic Publishing.

Moreira, L., Fossen, T. I., and Soares, C. G. (2007). Path following control system for a tanker ship model. In *J. Ocean Eng.*, 34(14–15), 2074–2085.

Pettersen, K.Y. and Lefeber, E. (2001). Way-point tracking control of ships. In *Proc. of the 40th IEEE Conference on Decision and Control,* 940–945.

Sujit, P.B., Saripalli, S., and Sousa, J.B. (2014). Unmanned aerial vehicle path following: a survey and analysis of algorithms for fixed-wing unmanned aerial vehicles. *IEEE Trans. on Control Systems Magazine*, 34(1), 42–59.

2017-07-31

A switching LOS guidance with relative kinematics for path-following of underactuated underwater vehicles

Abdurahman, Bilal

Elsevier

Abdurahman B, Savvaris A, Tsourdos A. (2017) switching LOS guidance with relative kinematics for path-following of underactuated underwater vehicles. IFAC-PapersOnLine, Volume 50, Issue 1, 2017, pp. 2290-2295

https://doi.org/10.1016/j.ifacol.2017.08.228